Published in IET Microwaves, Antennas & Propagation
Received on 14th February 2012
doi: 10.1049/iet-map.2012.0089

ISSN 1751-8725

Radiation and absorption of waves emitted by a radial dipole in the presence of a layered dielectric sphere with a spherical screen

V.V. Radchenko[1,*] *R. Sauleau*[2] *A.I. Nosich*[1]

[1]*Institute of Radio-Physics and Electronics NASU, Kharkiv 61085, Ukraine*
[2]*IETR, Universite de Rennes 1, Rennes Cedex 35042, France*
[*]*Present address: Department of Mathematics, Kharkiv National Academy of Municiple Economy, Kharkiv 61002, Ukraine*
E-mail: alex@emt.kharkov.ua

Abstract: Considered is the problem of electromagnetic wave radiation and absorption in the presence of a two-layer lossy dielectric sphere partially covered with a metal screen and illuminated by an elementary electric dipole. To find the field, the authors expand it in terms of spherical functions and use the method of analytical regularisation to reduce the problem to a matrix equation with favourable features. This enables us to obtain the radiation and absorption characteristics in a wide range of parameter variations and compare the efficiencies of shielding by different screens of varying angular size. As the studied structure can be viewed as a model of a head phantom with a helmet, the presented analysis can be useful for a control of specific microwave absorption rate levels.

1 Introduction

In recent years, numerous publications have appeared presenting the results of both experimental measurements and various numerical simulations of the electromagnetic wave absorption in mobile-phone user head phantoms [1–5]. These works considered head phantoms of many different shapes and degrees of complexity, from a primitive homogeneous cube to extremely detailed non-homogeneous copies of realistic heads. Spherically layered head models played an important role at the early stage of research [6–10] and dealt with both plane-wave illumination [6, 7] and excitation by localised sources (i.e. dipoles) [8–10]. These two cases are quite different and each of them is important for applications.

From the published results, one may notice that highly inhomogeneous models closely reproducing the real head are mandatory when studying the fine structure of the power absorption. However, the shape precision has rather little effect on the total absorbed power, apparently because the communication wavelength is similar to or greater than the head size and hence no resonances take place (additionally, they would be damped by the high losses). The estimations of the total power absorbed in the head of a phone user vary from 0.1 to 0.3 W [1–5]. Here, a major role is played by the head tissues volume and material parameters, that is, the static dielectric permittivity and the conductivity.

At the same time, there is no published study into the effect of a metal helmet on the overall electromagnetic power absorption. Such a study can be interesting, for example, in view of the frequent mounting of mobile communication antennas on the gear of emergency or rescue personnel. Therefore in this paper we simulate a human head capped with a metal helmet and illuminated by a short wire antenna (Fig. 1) by considering a layered lossy dielectric sphere partially covered with a metallic spherical screen; the excitation current is an elementary dipole located on the axis of symmetry above the screen. The time dependence is assumed to be $e^{-i\omega t}$.

From the viewpoint of modelling, this geometry is quite challenging. Typically similar problems are attacked with brut-force finite-difference time-domain codes whose convergence is not uniformly guaranteed and whose application in open-geometry problems leads to huge numerical efforts even if an electrically small scatterer is considered. In contrast, we fully exploit the simple shape of a spherical phantom by using the spherical-wave expansions and the method of analytical regularisation (MAR) [11], which provide fast and uniform point-wise convergence of the numerical solution and has controlled computational error. In the core of MAR there is the analytical inversion of the most singular part of the full-wave scattering operator. In our case it is the part associated with the static limit for a single zero-thickness perfectly electrically conducting (PEC) spherical screen in free space [12]. This method has also been applied in [13] to the analysis of the scattering of the plane wave incident along the axis of revolution of a partially screened homogeneous dielectric sphere.

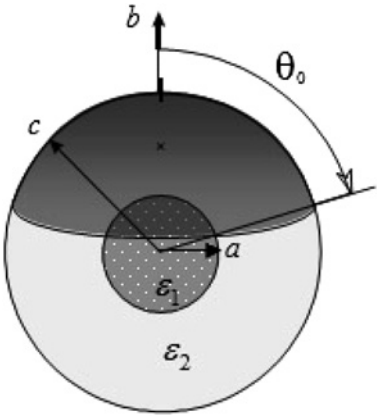

Fig. 1 *Two-layer dielectric sphere covered with a spherical PEC screen and excited with an elementary electric dipole*

More recently, the radiation characteristics of axisymmetrically excited PEC spherical-circular microstrip antennas with full and partial spherical PEC ground conductors were studied with MAR in [14, 15], respectively. Here we apply the same approach to the study of electromagnetic wave absorption in a layered head phantom and its reduction owing to a metal helmet. Therefore we refer to [14, 15] for the mathematical details and validation of the technique used and concentrate on the study of the wave absorption.

The rest of the paper is organised as follows. Section 2 contains a description of the phantom and helmet model and a brief mathematical formulation of the scattering problem. In Section 3, we reduce this problem to the dual-series equations and further, using MAR, to a Fredholm second kind infinite-matrix equation. Section 4 contains numerical results for the power absorbed in the head phantom with and without a protective helmet. This is followed by conclusions.

2 Model and formulation

The geometry of the considered structure is shown in Fig. 1. A double-layer dielectric spherical phantom has an inner layer radius a and an outer radius c. The choice of only two layers is based on the observation that, although one can distinguish three and more basic head tissues such as skin, bone and brain, the total thickness of the skin and skull together is some 30–50 times smaller than the head size. In the computations, to model a human head we take the complex permittivity values of the phantom layers, $\tilde{\varepsilon}_{1,2} = \varepsilon_0\varepsilon_{1,2} + i\sigma_{1,2}/\omega$, close to electro-physical parameters of the brain (domain 1) and the values obtained by averaging those for the skin and bone in proportion 1:2 (domain 2). The surrounding medium is assumed to be free space. The metal helmet is a PEC zero-thickness spherical screen of the angular size $2\theta_0$ conformal to the outer surface of the layered sphere. A wire antenna is modelled by an elementary radial electric dipole (RED) shifted by the distance b from the centre of the sphere above the centre of the spherical disk. Therefore the whole geometry of the source and the scatterer is rotationally symmetric. Note that this is the only configuration that provides a rotationally symmetric radiation pattern, which has obvious advantages in the field conditions.

To satisfy the requirements of the uniqueness theorem, the electromagnetic field problem must include Maxwell's equations off the boundaries and material interfaces, tangential field component continuity conditions at $r = a$, dual or mixed conditions at $r = c$, the Silver–Muller radiation condition at $r \to \infty$ and the electromagnetic energy finiteness condition in any finite volume outside the source, including the vicinity of the spherical disk rim [13]. Note that the last condition determines the behaviour of the field components near the rim; this behaviour is often expressed as the Meixner condition.

3 Basic equations

In our analysis, we reduce the boundary-value problem to the dual series equations (DSE) in terms of the associated Legendre functions. Here, we follow all steps of [14] where a spherical-circular microstrip antenna was studied, excited axisymmetrically by an RED located between the patch and the spherical ground. The standard steps of MAR in spherical-disk problems are (i) extraction of the most singular part of the DSE, (ii) inversion of this part based on the Abel integral equation technique and (iii) numerical solution of the obtained infinite matrix equation of the Fredholm second kind, after its truncation to the order that guarantees the desired accuracy.

The series expansion of the scattered field in terms of the outgoing spherical wave functions, in the outer domain, is

$$E_\theta^{\mathrm{sc}} = \frac{-pZ_0}{4\pi k_0 b^2 r}\sum_{n=1}^{\infty}(2n+1)z_n\zeta_n'(k_0 r)P_n^1(\cos\theta) \qquad (1)$$

where $p = Il$ is the dipole electric moment (i.e. product of the current strength, I, and its length, l), $Z_0 = (\mu_0/\varepsilon_0)^{1/2}$ is the free-space impedance, k_0 is the free-space wavenumber, $\zeta_n(x) = (\pi x/2)^{1/2}H_{n+1/2}^{(1)}(x)$ are the spherical Hankel functions in Debye's notation with the prime denoting differentiation in argument, $P_n^1(\cos\theta)$ are the associated Legendre functions and z_n are the unknown expansion coefficients of the scattered electric field in the outer domain. Similar expansions are used for the other field components in each partial radial domain and for the incident field components in the outer domain.

The DSE are generated by the mixed boundary conditions at $r = c$: (i) $E_\theta = 0$ on the surface of PEC spherical disk and (ii) H_φ is continuous across the complementary surface of the outer layer of the dielectric sphere. On introducing new unknown coefficients and notations

$$\tilde{z}_n = z_n n(n+1)[\zeta_n(k_0 c) - \sqrt{\varepsilon_2}\zeta_n'(k_0 c)D_n] \qquad (2)$$

these DSE can be cast to the form similar to (24) and (25) of [14]

$$\sum_{n=1}^{\infty}[\tilde{z}_n(1-\delta_n) + 2^{-1}(1+\varepsilon_2)k_0 c(2n+1)\zeta_n(k_0 b)\psi_n'(k_0 c)] \times P_n^1(\cos\theta) = 0, \quad \theta \in [0,\ \theta_0)$$

$$\sum_{n=1}^{\infty}(2n+1)\left[\frac{\tilde{z}_n}{n(n+1)} + \alpha_n\right]P_n^1(\cos\theta) = 0, \quad \theta \in (\theta_0,\ \pi] \qquad (3)$$

doi: 10.1049/iet-map.2012.0089

Here, the following notations are used

$$\alpha_n = \zeta_n(k_0 b)\psi_n(k_0 c) - \sqrt{\varepsilon_2}\zeta_n(k_0 b)\psi_n'(k_0 c)D_n \tag{4}$$

$$D_n = \frac{\psi_n(k_2 c)A_n + \zeta_n(k_2 c)B_n}{\psi_n'(k_2 c)A_n + \zeta_n'(k_2 c)B_n} \tag{5}$$

$$\delta_n = 1 + \frac{(2n+1)}{n(n+1)}\frac{(1+\varepsilon_2)k_0 c}{2}\left[-\frac{\zeta_n(k_0 c)}{\zeta_n'(k_0 c)} + \sqrt{\varepsilon_2}D_n\right]^{-1} \tag{6}$$

$$\begin{aligned} A_n &= \psi_n(k_1 a)\zeta_n'(k_2 a) - \psi_n'(k_1 a)\zeta_n(k_2 a)\sqrt{\varepsilon_2/\varepsilon_1}, \\ B_n &= \psi_n(k_2 a)\psi_n'(k_1 a)\sqrt{\varepsilon_2/\varepsilon_1} - \psi_n'(k_2 a)\psi_n(k_1 a) \end{aligned} \tag{7}$$

$k_{1,2} = k_0(\varepsilon_{1,2})^{1/2}$ and $\psi_n(x) = (\pi x/2)^{1/2}J_{n+1/2}(x)$ are the spherical Bessel functions in Debye's notation.

After performing semi-inversion of the DSE (see [14, 15]), we obtain an infinite-matrix equation for unknown coefficients

$$\tilde{z}_m = \sum_{n=1}^{\infty}\tilde{z}_n\delta_n Q_{\mathrm{nm}}^{(1)}(\theta_0) + V_m, \quad m = 1, 2, \ldots \tag{8}$$

$$\begin{aligned} V_m = {} & \frac{1+\varepsilon_2}{2}k_0 c\sum_{n=1}^{\infty}(2n+1)\zeta_n(k_0 b)\psi_n'(k_0 c)Q_{\mathrm{nm}}^{(1)}(\theta_0) \\ & + \sum_{n=1}^{\infty}n(n+1)\alpha_n[\delta_n^m - Q_{\mathrm{nm}}^{(1)}(\theta_0)] \end{aligned} \tag{9}$$

$$\begin{aligned} Q_{\mathrm{mn}}^{(1)}(\theta_0) &= Q_{\mathrm{mn}}(\theta_0) - \frac{Q_{0n}(\theta_0)Q_{m0}(\theta_0)}{Q_{00}\theta_0)} \\ Q_{\mathrm{mn}}^{(1)}(\theta_0) &= \frac{\sin(n+m+1)\theta_0}{\pi(n+m+1)} + \frac{\sin(n-m)\theta_0}{\pi(n-m)} \end{aligned} \tag{10}$$

Equation (8) is of the Fredholm second kind provided that $b > c$, that is, the dipole does not touch the helmet. This guarantees convergence of the truncated equation solution to the exact one when taking the truncation order progressively larger, see [14, 15] for details.

In Fig. 2, we show the dependence of the computational error (the definition of that quantity can be found in [11, 14]) against the matrix truncation order, N.

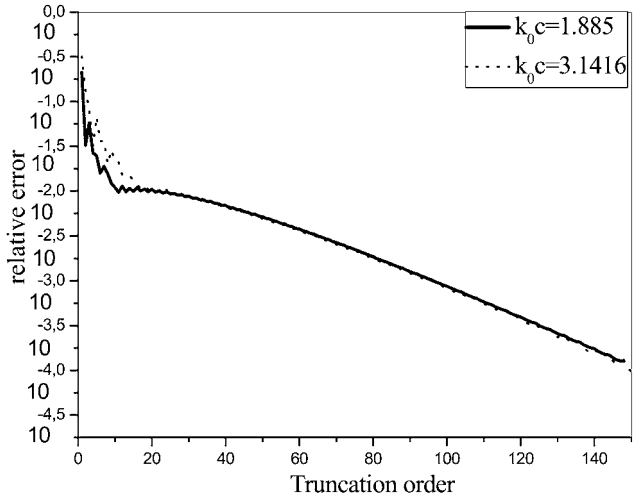

Fig. 2 *Computational error as a function of the matrix truncation number for $\theta_0 = 90^\circ$*

For the values of the other parameters, see the legend of Fig. 3

Here, two values of the normalised frequency, $k_0 c$, correspond to the phantom size and frequencies used when computing numerical results presented in the next section. One can see that some 100 unknowns are enough to provide three correct digits in $\{\tilde{z}_n\}_{n=0}^{N}$. For a further validation of our results, we have compared them with those computed using a different numerical method based on the Nystrom-type algorithm developed recently for the analysis of the scattering by rotationally symmetric PEC screens [16, 17]. The obtained normalised far-field radiation pattern (NRP) coincided with those presented below within the number of digits depended on the order of discretisation, as expected for two convergent algorithms in view of solution uniqueness.

After solving (8), one can calculate the electromagnetic field in the whole space making use of expressions like (1) and relations linking $\tilde{z}_n$ with the other expansion coefficients. This enables one to calculate the basic characteristics, which quantify the modification of radiation of the dipole antenna and absorption of its power in the partially screened double-layer dielectric sphere. They are the NRP, full power absorbed in the lossy-layered sphere, and the complete input resistance including radiation resistance and absorption resistance. For instance, the latter quantity is known to equal $R_{\mathrm{abs}} = 2\bar{P}_{\mathrm{abs}}/I^2$, that is proportional to the power absorbed inside the sphere

$$\begin{aligned} \bar{P}_{\mathrm{abs}} = {} & \frac{p^2 Z_0}{8\pi k_0 b^4}\mathrm{Re}\sum_{n=1}^{\infty}\frac{i\varepsilon_2^*}{k_2^*}(2n+1)(n+1)n[z_n\zeta_n(k_0 c) \\ & + \zeta_n(k_0 b)\psi_n'(k_0 c)][z_n\zeta_n'(k_0 c) + \zeta_n(k_0 b)\psi_n'(k_0 c)]^* D_n^* \end{aligned} \tag{11}$$

where * means the operation of complex conjugation. In computations, the summation in (11) is done over the terms corresponding to the truncation order N of (8).

4 Numerical results

In Fig. 3, we plot NRPs for two typical frequency values and three sizes of the PEC screen. The presence of the lossy sphere considerably distorts the far-field radiation pattern of a dipole even if the sphere diameter is smaller than the wavelength.

Electro-physical parameters of the spherical layers are taken from [1–10] and correspond to the human brain (for the inner domain) and the averaged in proportion 2:1 bone and skin (for the outer layer). As one can see, the presence of the head phantom considerably shifts the direction of the maximum radiation from the otherwise horizontal direction, that is, $\theta = 90^\circ$, to the lower half-space. The presence or absence of a helmet plays a minor role in this shift.

This is apparently because the relative values of both the real and imaginary parts of the complex-valued dielectric functions of the head tissues are very high. To prove this, we have computed the NRPs for the same RED-excited PEC 'helmets' located in free space (left column) and on top of the lossy sphere (right column), see Fig. 4. Even without a screen ($\theta_0 = 0$) the difference is quite significant. Adding a progressively larger helmet has little effect on the NRP of the heavily lossy sphere; however, it changes the NRP for the free-space case until two patterns coincide for the full PEC sphere ($\theta_0 = 180^\circ$).

Unlike the radiation pattern, the power absorbed in the sphere is a function of the near field. In Fig. 5, we give

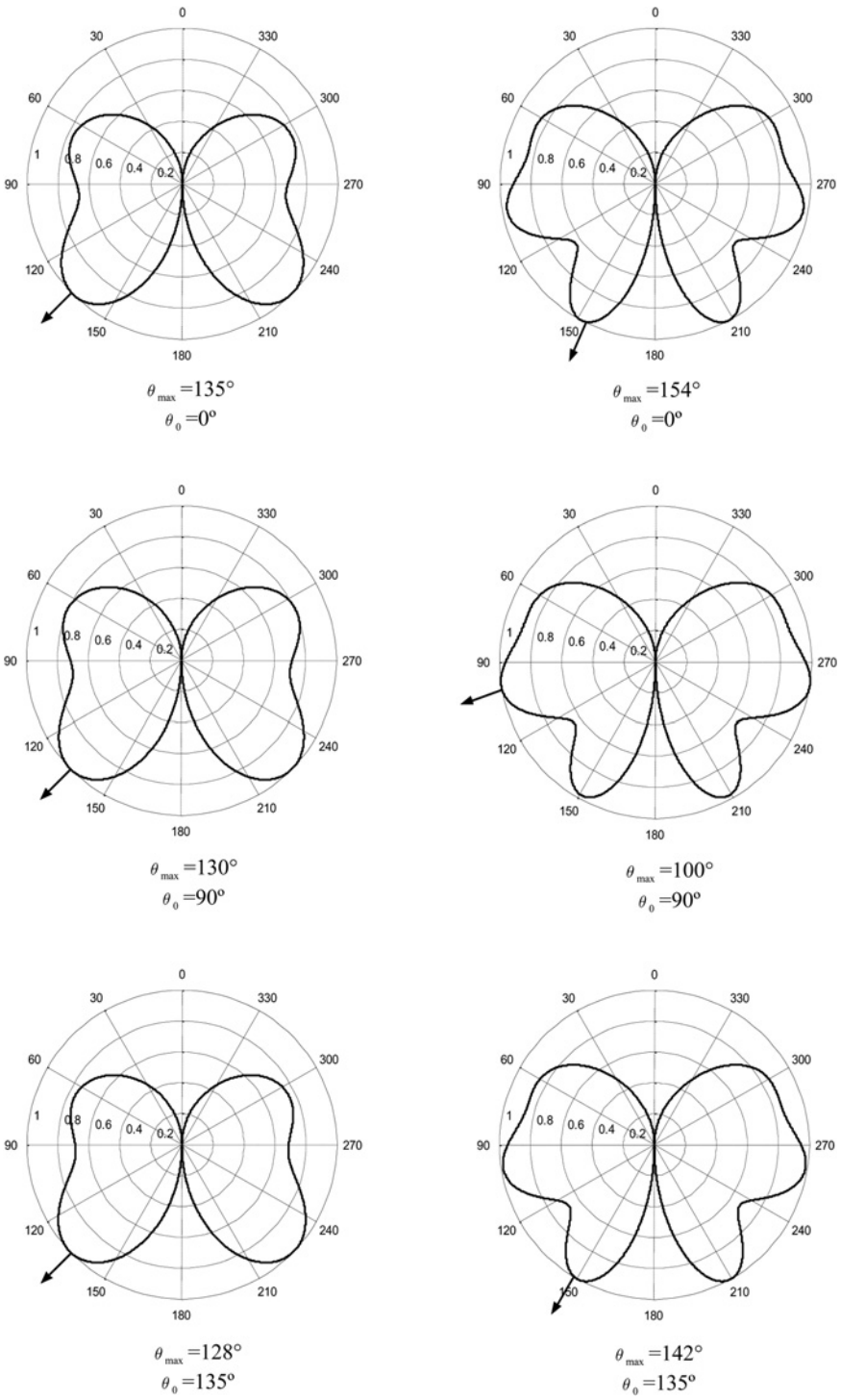

Fig. 3 *NRPs for an on-axis RED above a partially screened double-layer sphere at two frequencies typical for mobile communications, 900 MHz (left column) and 1500 MHz (right column)*

Sphere parameters: $c = 100$ mm, $c - a = 3$ mm, $\varepsilon_1 = 52.7$, $\sigma_1 = 1.05$ S/m, $\varepsilon_2 = 26.1$, $\sigma_2 = 0.45$ S/m at 900 MHz and $\varepsilon_1 = 46$, $\sigma_1 = 1.65$ S/m, $\varepsilon_2 = 26.1$, $\sigma_2 = 0.71$ S/m at 1500 MHz. Dipole parameters: current $I_0 = 0.1$ A, length $l = 20$ mm, shift $b - c = 20$ mm. θ_{max} is the direction of the maximum of NDR

numerical results showing both the radiation resistance (left scale) and the total radiated power (right scale) as a function of the frequency, for a bare sphere and three different spheres with 'helmets' of several angular sizes, θ_0. Here the layer permittivity and conductivity values are taken as average values between the known 900 and 1500 MHz data. This approximation can lead to some inaccuracy at the higher frequencies; however, it should not lead to significant errors. Note that we assume that the current in the dipole has fixed value (1 A) and hence the radiated and the absorbed powers are varying values proportional to the corresponding part of the total resistance.

Similar plots in Fig. 6 demonstrate the frequency dependence for the absorption resistance (left scale) and the total absorbed power (right scale). Comparison of these figures shows that two parts of the antenna input resistance are comparable to each other only for a bare sphere and low frequencies. If the frequency grows to the microwave-band values, the radiation resistance quickly overtakes the absorption resistance, which varies less dynamically.

doi: 10.1049/iet-map.2012.0089

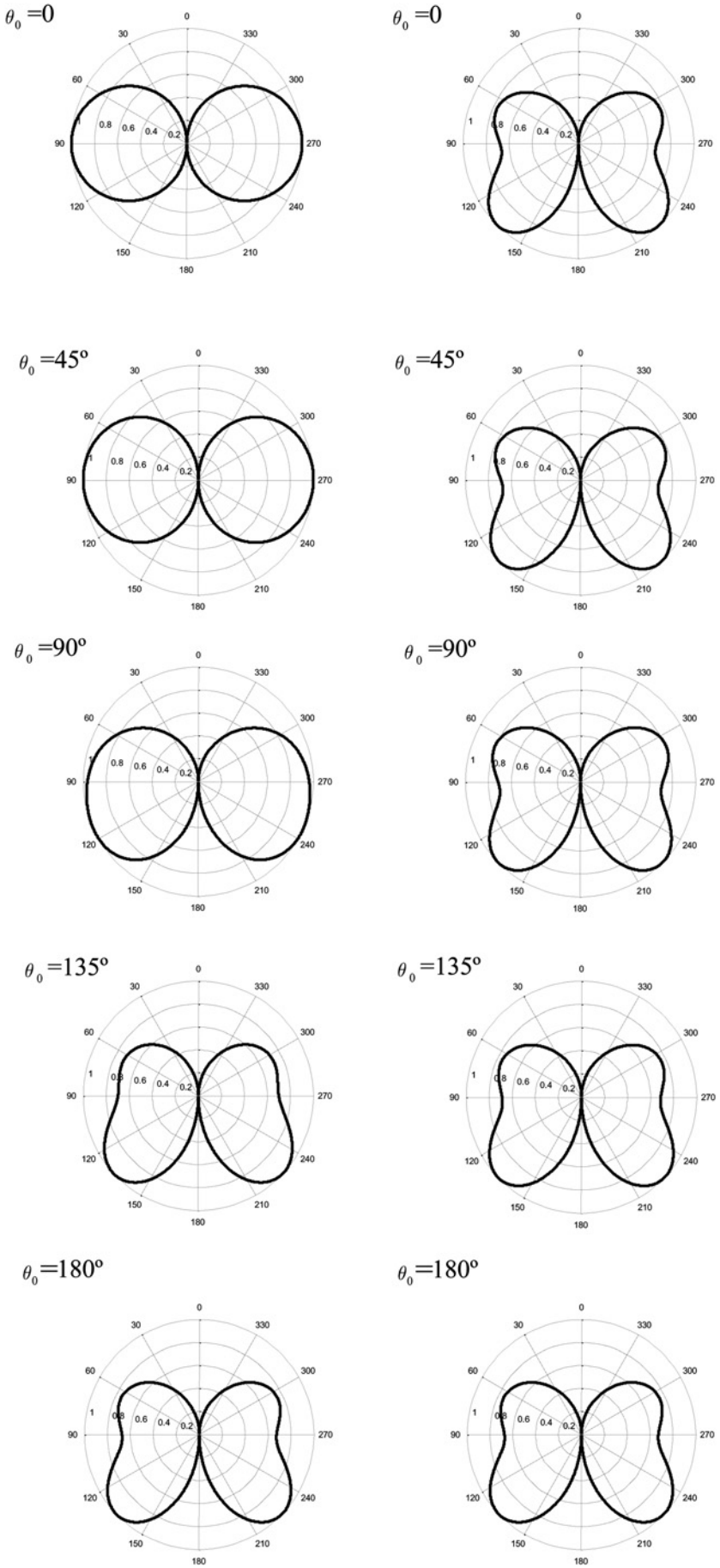

Fig. 4 *NRPs for on-axis RED over PEC spherical screens of indicated angular size located in free space (left column) and on the surface of a uniform dielectric sphere $c = 100$ mm, $c-a = 3$ mm, $\varepsilon_1 = 52.7$, and $\sigma_1 = 1.05$ S/m, at the frequency 900 MHz*

Other parameters are as in Fig. 3

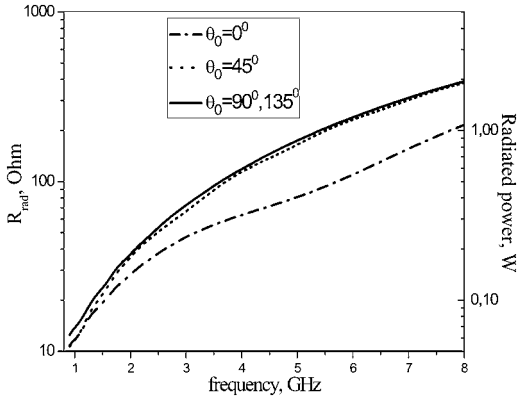

Fig. 5 *Radiation resistance (left scale) and radiated power (right scale) as a function of the frequency for the phantom, helmet and dipole antenna parameters indicated in the legend of Fig. 3*

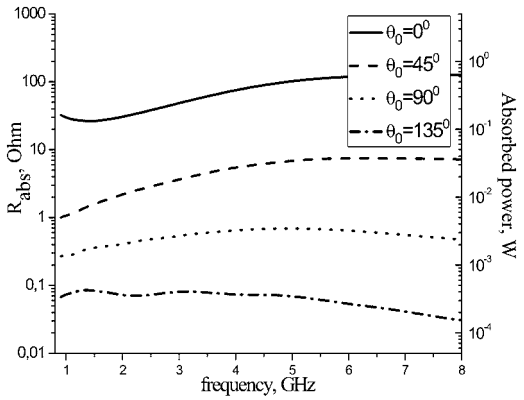

Fig. 6 *Absorption resistance (left scale) and absorbed power (right scale) as a function of the frequency for the phantom, helmet and dipole antenna parameters indicated in the legend of Fig. 3*

Adding a helmet to the head phantom lowers the absorption resistance to even smaller values.

Note that the results presented in Fig. 6 validate our choice of a simplified two-layer spherical head phantom, owing to the observation that at the communication frequencies of 900 and 1500 MHz the computed absorbed-power values are in good agreement with the data obtained using finite-difference methods and more sophisticated phantom models.

Namely, we find that the power absorbed in our model without the screen at 900 MHz is 120 mW, which is approximately the same as published in [1–5], although smaller than in [10] where a slightly larger head was assumed. Besides, these results show that a metal screen can effectively decrease the level of absorbed power. One can also see that the absorbed power function shows non-resonance behaviour in the whole range of considered frequencies. This can be explained by the high conductivity values and hence high bulk losses in the head tissues. Here, it can be reminded that the low-frequency 'dipole' resonance in the spherical-head-phantom absorption is observed at a lower frequency around 400–500 MHz and only under a plane electromagnetic wave illumination [7].

In Fig. 7, we show the dependence of the power absorbed in the considered simple head phantom as a function of the angular size θ_0 of the PEC helmet for the above-mentioned frequency values. When θ_0 varies, the most rapid change of

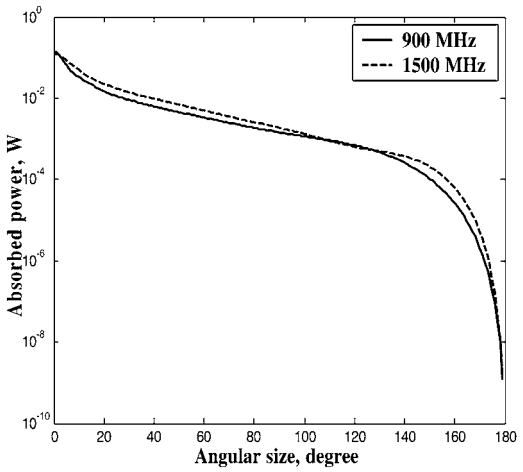

Fig. 7 *Absorbed power as a function of the screen angular half-width, θ_0, for the same geometrical and material parameters as in Fig. 3 and two values of the frequency, 900 and 1500 MHz*

absorption is observed for the small screens with $\theta_0 < 20^\circ$ and nearly full spherical screens with $\theta_0 > 150^\circ$.

A screen of some $\theta_0 = 20^\circ$ reduces absorption by 10 times, and a hemispherical helmet with $\theta_0 = 90^\circ$ reduces it in more than 100 times at the frequencies of mobile communication systems. In fact, according to Fig. 6, a similar reduction takes place in the very wide frequency band from 0.8 to 8 GHz and apparently beyond.

5 Conclusions

We have applied the accurate and computationally cheap MAR method for investigating the problem of electromagnetic wave absorption in a concentrically layered partially screened dielectric sphere fed with an electric dipole, as a simplified model of a helmet-equipped head with a dipole antenna. This has enabled us to study the dependence of the total amount of power absorbed in the head on the frequency and the helmet size, with guaranteed convergence. We have found that a hemispherical helmet reduces the absorbed power by a factor of 100 at the frequencies of today's mobile phones. The obtained results can be useful, for example, in the design of the mobile communication devices and for choosing the optimal sizes of screens necessary to reduce the absorption of microwaves in biological objects to the desired safe levels. They can also be taken as a reference for independent validation and accuracy assessment of general-purpose commercial and in-house numerical techniques.

6 References

1 Okoniewski, M., Stuchly, M.A.: 'A study of the handset antenna and human body interaction', *IEEE Trans. Microw. Theory Tech.*, 1996, **44**, (10), pp. 1855–1864

2 Hombach, V., Meier, K., Burkhardt, M., Kuhn, E., Kuster, N.: 'The dependence of EM energy absorption upon human head modeling at 900 MHz', *IEEE Trans. Microw. Theory Tech.*, 1996, **44**, (10), pp. 1865–1873

3 Bernardi, P., Cavagnaro, M., Pisa, S., Piuzzi, E.: 'Specific absorption rate and temperature increases in the head of a cellular-phone user', *IEEE Trans. Microw. Theory Tech.*, 2000, **48**, (7), pp. 1118–1126

4 Chen, H.-Y., Yang, H.-P.: 'SAR affected by shapes and electrical properties of the human head exposed to a cellular phone', *Microw. Opt. Technol. Lett.*, 2004, **42**, (1), pp. 1–4

5 Pisa, S., Cavagnaro, M., Lopresto, V., Piuzzi, E., Lovisolo, G.A., Bernardi, P.: 'A procedure to develop realistic numerical models of

doi: 10.1049/iet-map.2012.0089

cellular phones for an accurate evaluation of SAR distribution in the human head', *IEEE Trans. Microw. Theory Tech.*, 2005, **53**, (4), pp. 1256–1265
6 Shapiro, A.R., Lutomirski, R.F., Yura, H.T.: 'Induced fields and heating within a cranial structure irradiated by an electromagnetic plane wave', *IEEE Trans. Microw. Theory Tech.*, 1971, **19**, (2), pp. 187–196
7 Joines, W.T., Spiegel, R.J.: 'Resonance absorption of microwaves by the human skull', *IEEE Trans. Biomed. Eng.*, 1974, **21**, (1), pp. 46–48
8 Hizal, A., Baykal, Y.K.: 'Heat potential distribution in an inhomogeneous spherical model of a cranial structure exposed to microwaves due to loop or dipole antennas', *IEEE Trans. Microw. Theory Tech.*, 1978, **26**, (8), pp. 607–612
9 Skaropoulos, N.C., Ioannidou, M.P., Chrissoulidis, D.P.: 'Induced EM field in a layered eccentric spheres model of the head: plane-wave and localized source exposure', *IEEE Trans. Microw. Theory Tech.*, 1996, **44**, (10), pp. 1963–1973
10 Nikita, K.S., Stamatakos, G.S., Uzunoglu, N.K., Karafotias, A.: 'Analysis of the interaction between a layered spherical human head model and a finite-length dipole', *IEEE Trans. Microw. Theory Tech.*, 2000, **48**, (11), pp. 2003–2013
11 Nosich, A.I.: 'The method of analytical regularization in the wave-scattering and eigenvalue problems: foundations and review of solutions', *IEEE Antennas Propag. Mag.*, 1999, **41**, (3), pp. 34–49
12 Vinogradov, S.S.: 'A soft spherical cap in the field of a plane sound wave', *USSR J. Comput. Math. Math. Phys.*, 1978, **18**, (5), pp. 244–249
13 Vinogradov, S.S., Sulima, A.V.: 'Calculation of the Poynting vector flux through a partially screened dielectric sphere', *Radiophys. Quantum Electron.*, 1987, **32**, (2), pp. 160–166
14 Radchenko, V.V., Nosich, A.I., Daniel, J.-P., Vinogradov, S.S.: 'A conformal spherical-circular microstrip antenna: axisymmetric excitation by an electric dipole', *Microw. Opt. Technol. Lett.*, 2001, **26**, (3), pp. 176–182
15 Rondineau, S., Nosich, A.I., Daniel, J.-P., Himdi, M., Vinogradov, S.S.: 'MAR-based analysis of a spherical-circular printed antenna with a finite ground excited by an axially-symmetric probe', *IEEE Trans. Antennas Propag.*, 2004, **52**, (5), pp. 1270–1280
16 Balaban, M.V., Smotrova, E.I., Shapoval, O.V., Bulygin, V.S., Nosich, A.I.: 'Nystrom-type techniques for solving electromagnetics integral equations with smooth and singular kernels', *Int. J. Numer. Model. Electron. Netw. Devices Fields*, 2012, **25**, doi: 10.1002/jnm.1827 (to be published)
17 Bulygin, V.S., Nosich, A.I., Gandel, Y.V.: 'Nystrom-type method in three-dimensional electromagnetic diffraction by a finite PEC rotationally symmetric surface', *IEEE Trans. Antennas Propag.*, 2012, **60**, (#AP-1106-0686)